量子ドットの生物・医療応用

国立国際医療センター　山本健二

半導体ナノ粒子は、量子サイズ効果によって、強力な蛍光を出すことが特性を持つため細胞内レベルから生体レベルまで、その動体を追跡することが可能である。この特性により、薬物に結合された半導体ナノ粒子を体外からも追跡することも可能であり、副作用や安全性について個人レベルで詳しく検討することができる。本研究は、半導体ナノ粒子を用いて薬物や遺伝子の伝達システム開発研究である。またそれに伴い、半導体などナノ粒子の細胞毒性などの安全性について検討すると同時に一桁ナノ粒子の持つ量子サイズ効果による発光する蛍光ナノプローブを医療用に応用し、更に安全なナノ粒子を設計・製造することを目的としている。これまで開発したシリコンドットは、その一つの候補として可能性を持つ。

本研究は、5年間のナノメデシン指定研究として得た知見や成果を土台に臨床の現場で利用できる薬剤キャリアーおよびその医療技術開発を目指している。これまでに我々は、特異的な表面加工を開発し、生きた細胞の核、ミトコンドリア、ライソゾーム、細胞質、細胞膜への半導体ナノキャリアー伝達に成功している。本研究では、臓器特異的、細胞特異的、更に細胞小器官特異的薬剤伝達システムを開発する。

またこれまでにモデル薬物として抗圧剤を半導体ナノ粒子に結合させ家族性高血圧ラットを用いたモデル実験に成功した（Manabe et.al. IEEE Trans. BioNanoSci. 2006）。本研究ではモデル薬物として20種類の薬物を検討している様々な疾患に対する評価を行う（初年度は7種類検討）。それに伴いモデル薬物を体外から、その動態や局在性を観測する技術の開発に着手し、薬剤副作用の解析に使用可能なシステムを開発する。予備実験の一部は、日本経済新聞に2006年7月発表した。

さらに本研究では、非リンパ球免疫細胞の細胞伝達システムの開発行う。これまでに腹腔マクロファージがケモカインの一つであるCCL1によって活性化し、腹膜内皮細胞との凝集体を構成し、一つには消化器潰瘍の治癒に役立ち、他方では術後癒着を誘導することが、半導体ナノ粒子によって判明した（Hoshino et.al. J. of Immunology 2006）。本研究初年度では、レセプター抗体などを用いさらに術後癒着を阻止する方法を開発し、疾病治療効果の向上を図りたい。さらに本研究は、破骨細胞による骨融解、好中球による急性糸球体腎炎、川崎病にも同様な現象が見られる。そこで破骨細胞による歯髄炎、骨融解、活性化好中球による腎不全や冠動脈の血管炎の診断・治療への応用を行う（破骨細胞について初年度はプレート上で培養細胞を用いて行う）。

本研究における薬剤伝達システムおよび細胞伝達システムの研究成果により、直接的に副作用の軽減、治療効果の向上、疾病治療にあたってQOLの向上を実現できると考えている。

雑誌

発表者氏名	論文タイトル名	発表誌名	巻号	ページ	出版年
Shiohara A, Manabe N, Omata K, Yamamoto K.	ovel Surface Processing with Sulfonic Acid for Quantum Dot and Its Characteristics.	Journal of Chemical Engineering of Japan	39(1)	52-56	2006
Yamamoto S, Manabe N, Fujioka K, Hoshino A, Yamamoto K.	Visualizing Vitreous using Quantum Dots as Imaging Agents.	IEEE Transactions on NanoBioscience	3(6)	94-98	2007
Manabe N, Hoshino A, Liang YQ, Goto T, Kato N, Yamamoto K	Quantum dot conjugated with medicine as the drug tracer in vitro and in vivo.	IEEE Transactions on NanoBioscience	5(4)	263-267	2006
YamaFutamura Y, Yahara K, Yamamoto	Evidence for the production of fluorescent pyradine delivertives using supercritical water.	The Journal of Supercritical Fluids			2007 (in press)
1. A Hoshino, Y-I Kawamura, M Yasuhara, N Toyama-Sorimachi, K Yamamoto, A Matsukawa, S A. Lira,	Inhibition of CCL1-CCR8 interaction prevents aggregation of macrophages and development of	J. Immnol.			2007 (in press)
Yasugi E, Horiuchi A, Uemura I, Okuma E, Nakatsu M, Saeki K, Kamisaka Y, Kagechika H, Yasuda K, Yuo A	Peroxisome proliferator-activated receptor γ ligands stimulate myeloid differentiation and lipogenensis in the human leukemia NB4 cells.	Dev Growth Differ	48	177-188	2006
J. Jo, N. Nagaya, Y. Miyahata, M. Kataoka, M. Harada-shiba, K. Kangawa, Y. Tabata	Transplantation of genetically engineered mesenchymal stem cells improves cardiac function in rats with myocardial infarction: benefit of a novel nonviral vector, cationized dextran	Tissue Engineering			2007 (in press)
I. Ichi, K. Nakahara, Y. Miyashita, A. Hida-ka, S. Kutsukake, K. Inoue, T. Maruyama, Y. Miwa, M. Harada-Shiba, M. Tsushima, S. Kojo and Ki-sei Cohort Study	Association of ceramides in human plasma with risk factors of atherosclerosis	Lipids	41(9)	859-863	2006
A. Yamamoto, M. Harada Shiba, M. Endo, N. Kusakabe, T. Tanioka, H. Kato, and T. Sho-ji	The effect of ezetimibe on serum lipids and lipoproteins in patients with homozygous familial hypercholesterolemia under-going LDL-apheresis therapy	Atherosclerosis	186(1)	126-131	2006

Ochiya T, Honma K, Takeshita F, Nagahara S	Atelocollagen-mediated Drug Discovery Technology	Expert Opin. Drug Discov	2	159-167	2007
Hanai K, takeshita F, Honma K, nagahara S, maeda M, Minakuchi Y, Sano A, Ochiya T	Atelocollagen-mediated systemic DDS for nucleic acid medicines	Ann N Y Acad Sci.	1082	9-17	2006
Kurokawa Y, Honma K, Takemasa I, Nakamori S, Kita-Matsuo H, Motoori M, Nagano H, Dono K, Ochiya T, Monden M, Kato K.	Central genetic alterations common to all HCV-positive, HBV-positive and non-B, non-C hepatocellular carcinoma: A new approach to identify novel tumor markers	Int J Oncol.	28	383-391	2006
Banas A, Teratani T, Yamamoto Y, Tokuhara M, Takeshita F, Quinn G, Okochi H, Ochiya T.	Adipose tissue-derived mesenchymal stem cells as a source of stem cells for liver regeneration	Hepatology			(in press)
Takeshita F, Kodama M, Yamamoto H, Ikarashi Y, Ueda S, Teratani T, Yamamoto Y, Tamatani T, Kanegasaki S, Ochiya T, Quinn G.	Streptozotocin-induced partial beta cell depletion in nude mice without hyperglycaemia induces pancreatic morphogenesis in transplanted embryonic stem cells	Diabetologia	49	2948-2958	2006
Fujii T, Saito M, Iwasaki E, Ochiya T, Takei Y, Hayashi S, Ono A, Hirao N, Nakamura M, Kubushiro K, Tsukazaki K, Aoki D.	Intratumor injection of small interfering RNA-targeting human papillomavirus 18 E6 and E7 successfully inhibits the growth of cervical cancer	Int J Oncol.	29	541-548	2006
Kosaka N, Kodama M, Sasaki H, Yamamoto Y, Takeshita F, Takahama Y, Sakamoto H, Kato T, Terada M, Ochiya	FGF-4 regulates neural progenitor cell proliferation and neuronal differentiation	FASEB J.	20	1484-1485	2006
Banas A, Quinn G, Yamamoto Y, Teratani T and Ochiya T.	"Stem cells into liver" basic research and potential clinical applications	Adv Exp Med Biol.	Vol. 585	3-17	2006

Yanagihara K, Takigahira M, Takeshita F, Komatsu T, Nishio K, Hasegawa F, Ochiya, T.	A new photon counting technique for quantitatively evaluating progression of peritoneal tumor dissemination	Cancer Res.	66	7532-7539	2006
Katsumoto T, Aikawa Y, Iwama A, Ueda S, Ichikawa H, Ochiya, T, Kitabayashi I.	MOZ is essential for maintenance of hematopoietic stem cells.	Genes & Dev.	20	1321-1330	2006
Takeshita F, Ochiya T.	Therapeutic potential of RNA interference against cancer	Cancer Sci.	97	689-696	2006
Fukaya M, Isohata N, Ohta H, Aoyagi K, Ochiya T, Nakanishi Y, Taniguchi H, Sakamoto H, Shimoda T, Nimura Y, Yoshida T, Sasaki H.	Hedgehog signal activation in gastric pit cell and in diffuse type gastric cancer	Gastroentero logy	131	14-29	2006
Fukasawa M, Morita S, Kimura M, Horii T, Ochiya T, Hatada I,	Genomic imprinting in Dicer1-hypomorphic mice	Cytogenet Genome Res.	113	138-143	2006
Ueda S, Fukamachi K, Matsuoka Y, Takasuka N, Takeshita F, Naito A, Iigo M, Alexander DB, Moore MA, Saito I, Ochiya T, Tsuda H.	Ductal origin of pancreatic adenocarcinomas induced by conditional activation of a human Ha-ras oncogene in rat pancreas	Carcinogenes is	27	2497-2510	2006
J. S. Park, Y. Akiyama, Y. Yamasaki, K. Kataoka	Preparation and characterization of polyion complex micelles with a novel thermo-sensitive poly(2-isopropyl -2-oxazoline) shell via the complexation of oppositely charged block ionomers	Langmuir	23 (1)	138-146	2007

Arnida, N. Nishiyama, N. Kanayama, W. -D. Jang, Y. Yamasaki, K. Kataoka	PEGylated gene nanocarriers based on block catiomers bearing ethylenediamine repeating units directed to remarkable enhancement of photochemical transfection	J. Control. Release	115 (2)	208 215	2006
J. S. Park, K. Kataoka	Precise control of lower critical solution temperature of thermosensitive poly(2-isopropyl-2-oxazoline) via gradient copolymerization with 2-ethyl-2-oxazoline as a hydrophilic comonomer	Macromolecules	39 (19)	6622-6630	2006
N. Nishiyama, Arnida, W. -D. Jang, K. Date, K. Miyata, K. Kataoka	Photochemical enhancement of transgene expression by polymeric micelles incorporating plasmid DNA and dendrimer-based photosensitizer	J. Drug Target	14 (6)	413-424	2006
W. -D. Jang, Y. Nakagishi, N. Nishiyama, S. Kawauchi, Y. Morimoto, M. Kikuchi, K. Kataoka	Polyion complex micelles for photodynamic therapy: incorporation of dendritic photosensitizer excitable at long wavelength relevant to improved tissue-penetrating property.	J. Control. Release	113 (1)	73-79	2006
W. Kim, Y. Yamasaki, K. Kataoka	Development of a fitting model suitable for the isothermal titration calorimetric curve of DNA with cationic ligands.	J. Phys. Chem. B	110 (22)	10919-10925	2006
A. Koide, A. Kishimura, K. Osada, W. -D. Jang, Y. Yamasaki, K. Kataoka	Semipermeable polymer vesicle (PICsome) self-assembled in aqueous medium from a pair of oppositely charged block copolymers: physiologically stable micro-/nano- containers of water-soluble macromolecules.	J. Am. Chem. Soc.	128 (18)	5988-5989	2006

M. M. Ali, M. Oishi, F. Nagatsugi, K. Mori, Y. Nagasaki, K. Kataoka, S. Sasaki	Intracellular inducible alkylation system that exhibits antisense effects with greater potency and selectivity than the natural oligonucleotide.	Angew. Chem. Int. Ed.	45 (19)	3136-3140	2006
M. Oishi, K. Kataoka, Y. Nagasaki	pH-responsive three-layered PEGy- lated polyplex micelle based on a lactosylated ABC triblock copolymer as a targetable and endosome-disruptive nonviral gene vector.	Bioconjugate Chem.	17 (3)	677-688	2006
Y. Kakizawa, S. Furukawa, A. Ishii, K. Kataoka	Organic-inorganic hybrid-nanocarrier of siRNA constructing through the self-assembly of calcium phosphate and PEG-based block aniomer.	J. Control. Release	111 (3)	368-370	2006
M. M. Ali, M. Oishi, F. Nagatsugi, K. Mori, Y. Nagasaki, K. Kataoka, S. SasakiN. Kanayama, S. Fukushima, N. Nishiyama, K. Itaka, W. -D. Jang, K. Miyata, Y. Yamasaki, U. -I. Chung, K.	A PEG-based biocompatible block catiomer with high buffering capacity for the construction of polyplex micelles showing efficient gene transfer toward primary cells.	ChemMedChem	1 (4)	439-444	2006
Satoru Yamamoto, Noriyoshi Manabe, Kouki Fujioka, Akiyoshi Hoshino, and Kenji Yamamoto	Visualizing Vitreous Using Quantum Dots as Imaging Agents	IEEE Transactions on Nanobioscien ce	Vol. 6, No. 1	94-98	2007
Akiyoshi Hoshino, Tomokazu Nagao, Toshiko Ito-Ihara, Akiko Ishida-Okawara, Kazuko Uno, Eri Muso, Noriko Nagi-Miura, Naohito Ohno, Kazuhiro Tokunaka, Shiro Naoe, Hiroshi Hashimoto, Masato Yasuhara, Kenji Yamamoto, **Kazuo**	Trafficking of QD-conjugated MPO-ANCA in Murine Systemic Vasculitis and Glomerulonephritis model mice	Microbiol. Immunol	in press		2007

Akiko Ishida-Okawara, Noriko Nagi-Miura, Toshiaki Oharaseki, Kei Takahashi, Akinori Okumura, Hitoshi Tachikawa, Shin-ichiro Kashiwamura, Haruki Okamura, Naohito Ohno, Hidechika Okada, Peter.	Neutrophil activation and induced by *C. albicans* water-soluble mannoprotein-β-glucan complex (CAWS)	Exp. Mol. Pathol	in press	77–87	2007
Tomokazu Nagao, Mimiko Matsumura, Ayako Mabuchi, Akiko Ishida-Okawara, Osamu Koshio, Haruyuki Minamitani, and **Kazuo Suzuki**	Up-regulation of adhesion molecule expression in glomerular endothelial cells by anti-myeloperoxidase antibody.	Neprol. Dialysis Transplant	22	1854-1861	2007
Shinohara Hiroyasu Nagai-Miura Noriko Ishibashi Ken-ichi, Adachi Yoshiyuki Akiko Ishida-Okawara, Toshiaki Oharaseki, Kei Takahashi, Shiro Naoe, **Kazuo Suzuki**, and Naohito	Beta-mannosyl linkages negatively regulate anaphylaxis and vasculitis in mice, induced by CAWS, fungal PAMPs composed of mannoprotein-beta-glucan complex secreted by Candida albicans.	Biol. Pharm. Bull.	29	1016-1022	2006
Shouichi Fujimoto, Shigehiro Uezono, Shuichi Hisanaga, Keiichi Fukudome, Shigeto Kobayashi, **Kazuo Suzuki**, Hiroshi Hashimoto, Hiroyuki	Incidence of ANCA-associated primary renal vasculitis in Miyazaki Prefecture: The first population-based, retrospective epidemiological survey in Japan.	Clinical Journal of American Society of Nephrology.	1	1291-1299	2006
Yasuaki Aratani, Fumiaki Kura, Haruo Watanabe, Hisayoshi Akagawa, Yukie Takano, Akiko Ishida-Okawara, **Kazuo Suzuki**, Nobuyo Maeda, and Hideki Koyama	Contribution of the myeloperoxidase-dependent oxidative system to host defense against *Cryptococcus neoformans* .	J. Med. Microbiol.	55	67-71	2006
A. S. Persad, Y. Kameoka, S. Kanda, Y. Niho, **K. Suzuki**	Found in a Japanese Patient with Complete Myeloperoxidase	Gene Expression	13	310-320	2006
N. Nagai-Miura, T. Harada, H. Shinohara, K. Kurihara, Y. Adachi, A. Ishida-Okawara, T. Oharaseki, K. Takahashi, S., Naoe, **K. Suzuki** and N. Ohno	Lethal and severe coronary arteritis in DBA/2 mice induced by fungal Pathogen, CAWS, *Candida albicans* water-soluble fraction	Atherosclerosis	186		2006

Novel Surface Processing with Sulfonic Acid for Quantum Dot and Its Characteristics

Amane SHIOHARA, Noriyoshi MANABE,
Kazumi OMATA and Kenji YAMAMOTO
Department of Medical Ecology and Informatics, Research Institute, International Medical Center of Japan, 21-1, Toyama 1, Shinjyuku-ku, Tokyo 162-8655, Japan

Keywords: QD-SO_3^-, Surface Processing, Sulfonic Acid, Acidic Conditions

We developed smaller sized quantum dots covered with sodium 2-mercaptoethanesulfonate which has a sulfonyl group (QDs-SO_3^-), and compared its stability in acid, salt and buffer solutions with that of the quantum dots covered with the mercaptoundecanoic acid (QDs-MUA) and covered with the NH_2 group (QDs-NH_2). We found that the QD-SO_3^- well disperses in these solutions without quenching and this stability holds on for 24 h. Next, we investigated the effect of Sheep Serum Albumin (SSA) coating. The SSA coating stabilizes the QD-MUA in the solutions. However, for the QD-SO_3^-, it does not have any significant effect. It implies that the QD-SO_3^- has advantages over the other quantum dots on the stability in the solutions. These results suggest that the novel surface processing using the sulfonyl group expands the possibilities of applications for various fields.

Introduction

The nanometer-size semiconductor is called a quantum dot (QD). The quantum dots are characterized by the following quantum effects: (1) a special photo quality caused by widening the band gap when the spatial dimension is reduced (Unold *et al.*, 2004; Weig *et al.*, 2004); (2) they can produce different colors by changing the sizes (Mattoussi *et al.*, 2000); and (3) they have excellent photostability and their fluorescences can be observed more than 1 h (Hoshino *et al.*, 2004). Because of these interesting characteristics, quantum dots are widely employed for industrial and medical applications. For the industrial applications, they are used as photovoltaics, multicolor LEDs, electronic memory devices, quantum dot barcodes, high throughput chemical and biological sensors (Han *et al.*, 2001; Coe *et al.*, 2002; Santori *et al.*, 2002; Zrenner *et al.*, 2002; Alivisatos., 2004; Clapp *et al.*, 2004). For the medical applications, they are coming into use as immunostaining, a drug delivery system, and so on (Dubertret *et al.*, 2002; Xu *et al.*, 2003; Shiohara *et al.*, 2004). Here, one of the indispensable properties for both applications is their interactions with other materials; especially the interaction with water plays a crucial role for the dispersibility in aqueous solutions. For example, this property is important for integrating quantum dots into devices functionally (Jaffer *et al.*, 2004). A simple way to control the solvation is to modify the surface of the quantum dots. The surface-modified quantum dots synthesized for the first time are covered with non-polar groups of organic molecules such as trioctyl phosphine oxide (TOPO), so that they are insoluble in water, putting some limitations on their functions in aqueous conditions. This problem was solved by Chan and Nie (1998). They synthesized water-soluble quantum dots, CdSe/QD-MUA, the surface of which are covered with mercaptoundecanoic acid (MUA). This QD-MUA was made by the method of substituting non-polar groups of organic molecules on the surface of quantum dots for MUA. The QD-MUA made a tremendous contribution to the possibility of application of quantum dots for various fields not only industry but also medical biology (Huang *et al.*, 1998; Åkerman *et al.*, 2002; Hanaki *et al.*, 2003; Gao *et al.*, 2004; Hoshino *et al.*, 2004; Wu and Bruchez, 2004; Santra *et al.*, 2005).

A further important problem is that the QD-MUA is not stable in acid or it coheres easily in buffer solution. This should be an impediment to medical 3 applications, and it might also cause a problem in the field of industry. Hanaki *et al.* (2003) have succeeded to stabilize QD-MUA under physiological conditions by coating it with sheep serum albumin (SSA), and the purpose of the present work is to develop their study. We investigated CdSe/QD covered with sodium 2-mercaptoethanesulfonate (QD-SO_3^-) and focused on its compatibility with various solvents. The reasons we chose this ligand are as follows. First, the sulfonyl group is a strong acid, and secondly this ligand can be

Received on May 18, 2005. Correspondence concerning this article should be addressed to K. Yamamoto (E-mail address: backen@ri.imcj.go.jp).

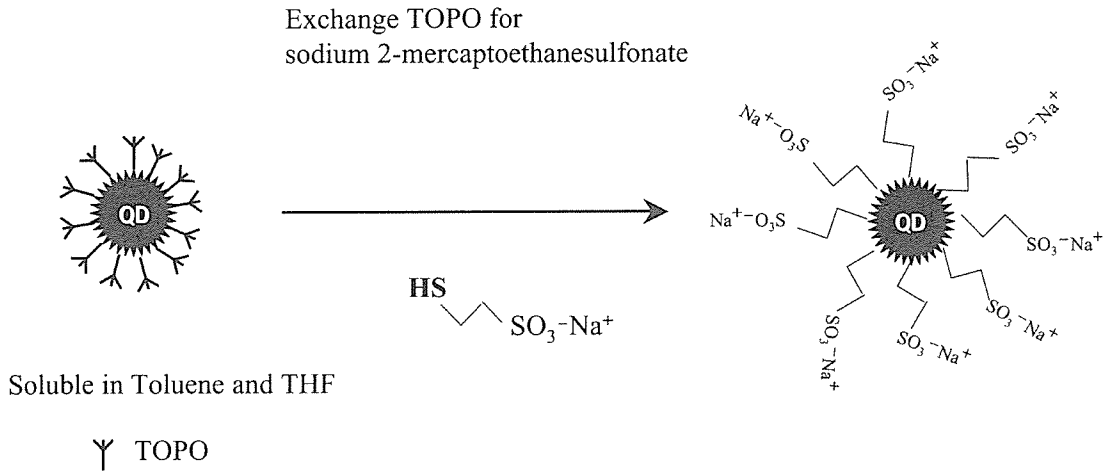

Fig. 1 Synthesis of QD-SO_3^-

connected with an alkyl chain followed by the terminal group, SH. In this study, (1) we succeeded in synthesis of QD-SO_3^- for the first time; (2) we compared the stability of QD-SO_3^- with that of quantum dots with NH_2 connected to two alkyl groups (QD-NH_2) and QD-MUA in acid and buffer solutions; and (3) we studied those quantum dots coated with SSA to conduct the experiments under conditions similar to Hanaki *et al.* (2003).

1. Materials and Methods

1.1 Preparation of QD-MUA, QD-NH_2 and QD-SO_3^-

The quantum dots with the core of CdSe and the shell of ZnS (see **Figure 1**) were synthesized from the QD-tri-*n*-octylphosphine oxide (QD-TOPO). After QD-TOPO (Murray *et al.*, 1993; Hines and Guyot-Sionnest, 1996; Peng *et al.*, 1997) dissolved in tetrahydrofuran (Wako Pure Chemical Industries, Ltd.), the solution was warmed up to 85°C, and sodium 2-mercaptoethanesulfonate (Shionogi & Co., Ltd.), MUA (Sigma-Aldrich Co.) and cysteamine hydrochloride (Wako Pure Chemical Industries, Ltd.) dissolved in ethanol were dripped into it. It was reflexed for 12 h. Then, for the sodium 2-mercaptoethanesulfonate and MUA, 100 μL of the NaOH solution (pH 10) was added into them to ionize the quantum dots, and the tetrahydrofuran was evaporated at 90°C. The unrefined quantum dots thus obtained, were refined and concentrated with an ultrafiltration membrane (Microcon YM-3, Millipore Corp.) and sephadex column (MicroSpin G-25 Columns, Amersham Bioscience Corp.), and then each of the refined quantum dot was obtained. To coat the quantum dots with SSA, we mixed the solutions of quantum dots and SSA.

1.2 Preparation of acid, buffer and salt solutions

The acidic conditions were provided by sulfuric acid. The observation range was 0.25 mM (pH 3.2)–0.001 mM (pH 5.1). The pH of borate buffer solution was pH 9. The concentration of the salt solutions were 1 M NaCl and 5 M NaCl. The PBS and MEM were used as salt solutions as well. The concentration of QD-MUA, QD-NH_2, and QD-SO_3^- was 0.1 mg/mL. As for these quantum dots, the powder of each quantum dot was weighed and 10 mg/mL aqueous solution was made. Then the solutions were diluted into 0.1 mg/mL. The quantum dots were added to each solution and they were observed 1 h and 24 h after.

Table 1 Particle size and surface potential of each quantum dot

	Particle size [nm]	Zeta potential [mV]
QD-SO_3	10.12	−32.74
QD-MUA	19.97	−32.31
QD-NH_2	10.36	10.95

The particle size and surface potential of each quantum dot was measured with Zetasizer (Malvern Instruments Ltd.) after filtration. A 0.45 μm filter was used for this experiment.

2. Result

2.1 Spectrum intensity, size distribution, and zeta potential

We measured the fluorescent intensity of QD-MUA, QD-NH_2, and QD-SO_3^-. The spectra are shown in **Figure 2**. The fluorescent peak intensity of QD-MUA was about 3 times as large as that of QD-SO_3^-. However, that of QD-NH_2 was 3 times lower than that of QD-SO_3^-.

The results of the particle sizes and the zeta potential are shown in **Table 1**. The particle diameter of QD-SO_3^- is 10.12 ± 3.247 nm. On the other hand, 80% of the provided QD-MUA have the particle diameter

Table 2 Stability of each quantum dot for acid, salts, base, and buffer

	QD-SO_3		QD-SO_3-SSA		QD-MUA		QD-MUA-SSA		QD-NH_2	
	1 h	o/n	1 h	o/n	1 h	o/n	1 h	o/n	1 h	o/n
Water	+	+	+	+	+	+	+	+	+	–
0.25 mM H_2SO_4/pH 3.2	+	–	+	+	q	q	+	–	q	q
0.1 mM H_2SO_4/pH 3.7	+	+	+	+	q	q	+	+	+	–
0.01 mM H_2SO_4/pH 4.6	+	+	+	+	+	+	+	+	+	–
Borate buffer/pH 9	+	+	+	+	+	–	+	+	+	+
1 M NaCl	+	+	+	+	–	–	+	–	–	–
5 M NaCl	+	+	+	+	–	–	+	–	q	q
PBS	+	+	+	+	–	–	+	–	–	–
MEM	+	+	+	+	–	–	+	+	+	–

+: dispersion, –: aggregation, q: quenching
Stabilities of each quantum dot for acid, salts, base, and buffer solutions were measured with 0.1 mg/mL of concentration of each quantum dot. And photos were taken after 1 h and overnight. o/n shows after overnight.

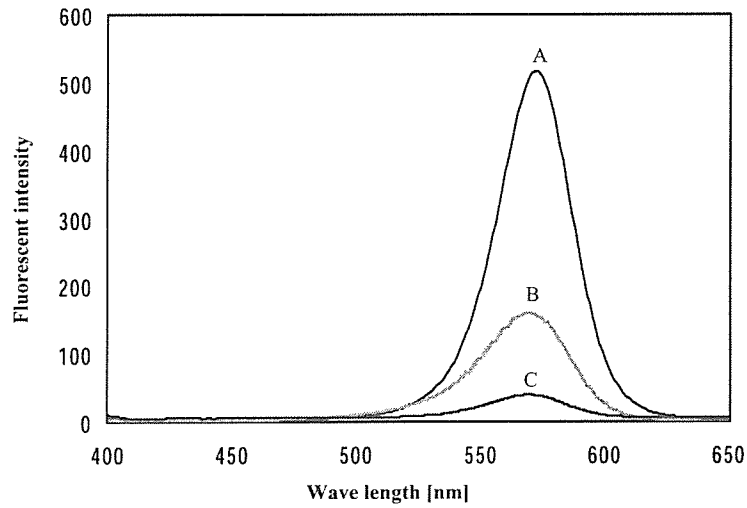

Fig. 2 Emission spectra of each quantum dot. Spectra A stands for QD-MUA, spectra B and spectra C stand for QD-SO_3^- and QD-NH_2 respectively. Each quantum dot was dissolved in distilled water and their emission spectra were measured with FP-6500. Each quantum dot was excited at 350 nm. Concentration of each quantum dot was 0.1 mg/mL

of 19.97 ± 6.563 nm. The diameter of the rest is 572 ± 418 nm but these particles probably aggregated in water. The diameter of QD-NH_2 is 10.36 ± 3.224 nm, which is almost the same size as that of QD-SO_3^-. The zeta potentials of QD-SO_3^-, QD-MUA and QD-NH_2 were –32.7, –32.3, and +10.95 mV, respectively. The results of these measurements were consistent with what we can predict from the structure of each quantum dot.

2.2 Stability in acid, salts, base, and buffer solution

The results about the stability of the quantum dots are summarized in **Table 2**. Here, the stability stands for the condition that quantum dots disperse and give off light in the solutions in this study. In acid, salt, and buffer solutions, the non-coat QD-SO_3^- is stable except the case of pH 3.2 after 24-h incubation. The SSA-coated QD-SO_3^- is always stable in all the solutions. The stability of the non-coated QD-MUA was quite low and quenching was occurred in acid (see **Figure 3**). The SSA-coated QD-MUA was stable under all the acidic conditions after 1-h incubation and in NaCl solutions as well in this experiment, but it aggregates at pH 3.2 and NaCl solutions after 24 h. The QD-NH_2 generally was not stable in all the solutions after 24 h.

3. Discussion

Our study is based on the prediction that QD-SO_3^- shows high stability in low pH solutions because this surface ligand is expected to be compatible with the sulfuric acid. Thus, let us compare the stability of QD-SO_3^-, QD-MUA and QD-NH_2 in detail.

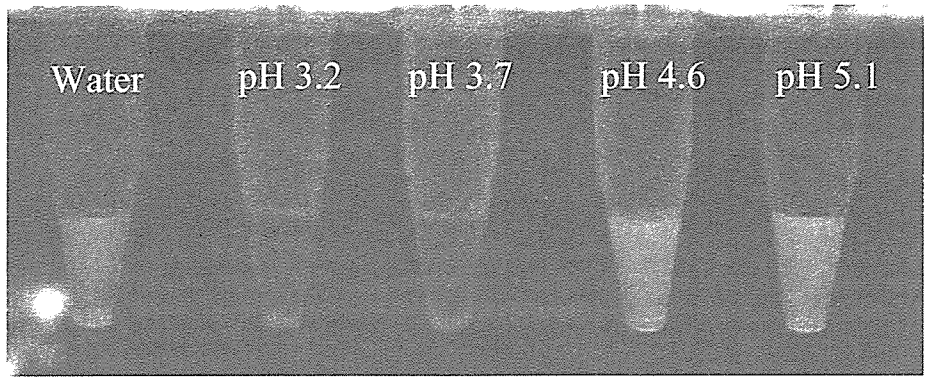

Fig. 3 Representative results of QD-MUA. Photos were taken after 24 h. The pictures stand for QD-MUA in water, acidic solutions of pH 3.2, 3.7, 4.6 and 5.1 from the left-hand side, respectively

Firstly, we compare the stability of the quantum dots without the SSA coating. Under acidic conditions, the QD-SO_3^- is more stable than the QD-MUA (see the second and third rows in Table 2). The QD-MUA undergoes quenching under the acidic conditions, pH 3.2 and pH 3.7. There are several possibilities for the reasons of the quenching: (1) the surface states of the quantum dots are changed by the acidic solvent; (2) the exciting energy is transformed to energy other than fluorescence; and (3) the ZnS shell of the quantum dot is destroyed by the acidic solvent. Among them, the last possibility is the most plausible because the quenching occurred rapidly when the quantum dots was added into the solvent. This quenching results from the fact that the sulfonyl group of QD-SO_3^- is more compatible with the sulfuric acid than the carboxyl group of the QD-MUA and the ZnS shell of the QD-SO_3^- can be protected. In addition, the hydrophobic alkyl group in the ligand of QD-MUA is longer than that of QD-SO_3^- so that the ligands might prevent each other from bonding to the surface of the quantum dot during the synthesis process. As a result, the number of surface ligands of the QD-MUA is smaller than that of the QD-SO_3^-, and the ZnS shell is easily attacked by the acidic molecules.

Also in the buffer and salt solutions, the non-coated QD-SO_3^- is more stable than the non-coated QD-MUA (see the fifth to ninth rows in Table 2). This is because the ionization of the sulfonyl group of the QD-SO_3^- is larger than the carboxyl group of the QD-MUA. Accordingly, the surface of QD-SO_3^- is not easily terminated by hydrogen and the polarity of the QD-SO_3^- can be kept in the buffer and salt solutions.

Secondly, we compare the SSA-coated and non-coated quantum dots and discuss the effect of the SSA coating. While Hanaki *et al.* (2003) have already reported that SSA raises the dispersibility of QD-MUA in MEM (see the last row in Table 2), we found that the same effect can be observed for the SSA-coated QD-MUA in acid and borate buffer as well. This result indicates that the SSA coating the surface of the quantum dots prevents the contact of the quantum dots each other, regardless of the kind of solvents. On the contrary, it is noteworthy that there is no remarkable difference between the SSA-coated QD-SO_3^- and no-coated QD-SO_3^-. For the QD-SO_3^-, SSA coating has no significant effect for the stability in acid, buffer, and salt solutions. This result implies that the QD-SO_3^- has a great advantage over the QD-MUA as for dispersion in solutions.

For industrial applications, SSA coating is not always needed because additional processes of the surface coating take one's time and the SSA must be denatured at high temperature. Concerning this point, the QD-SO_3^- coated with SSA has an important meaning for biological applications. The SSA coating has significant roles of carrying the quantum dots into cells, and without coating, they do not get inside cells (data not shown).

Finally, we mention an advantageous property of the QD-SO_3^-. The QD-SO_3^- has smaller particle size than the QD-MUA: the diameter of the QD-SO_3^- is about a half compared to QD-MUA. This means that the QD-SO_3^- is more suitable for the use in immunostaining.

It is desirable for industrial applications to determine the threshold of the stability against acids. For this purpose, the titration is a better way to give their exact values. We are about to perform such experiments in the future work.

Acknowledgment

We thank Dr. Richard Tilley at Victoria University in Wellington and Hideki Maruyama at Shionogi & Co., Ltd. for the important discussion and help. We were supported by Grants-in-Aid for the Advancement of Medical Equipment of the Ministry of Health, Labor and Welfare and Japan Association.

Literature Cited

Åkerman, M. E., W. C. W. Chan, P. Laakkonen, S. N. Bhatia and E. Ruoslahti; "Nanocrystal Targeting *in vivo*," *Proc. Natl. Acad. Sci. U.S.A.*, **99**, 12617–12621 (2002)

Quantum Dot as a Drug Tracer *In Vivo*

Noriyoshi Manabe, Akiyoshi Hoshino, Yi-qiang Liang, Tomomasa Goto, Norihiro Kato, and Kenji Yamamoto*

Abstract—**Quantum dots (QDs) have been applied to a wide range of biological studies by taking advantage of their fluorescence properties. There is almost no method to trace small molecules including medicine. Here, we used QDs for fluorescent tracers for medicine and analyzed their kinetics and dynamics. We conjugated QDs with captopril, anti-hypertensive medicine, by an exchange reaction while retaining the medicinal properties. We investigated the medicinal effect of QD-conjugated captopril (QD-cap) *in vitro* and *in vivo*. We also evaluated the concentration and the distribution of the QD-cap in the blood and the organs with their fluorescence. We demonstrate that the QD-cap inhibits the activity of ACE *in vitro*. The QD-cap reduced the blood pressure of hypertensive model rats. The concentration of the QD-cap in the blood was measured by using the standard curve of the fluorescence intensity. The blood concentration of the QD-cap decrease exponentially and QD-cap has approximately the same half-life as that of captopril. In addition, the fluorescence of the QDs revealed that QD-cap accumulates in the liver, lungs, and spleen. We succeeded in analyzing the dynamics and kinetics of small molecules using fluorescence of QDs.**

Index Terms—**Anti-hypertensive drug, distribution in organs, measurement of the concentration in blood, quantum dot conjugated with medicine.**

I. Introduction

CERTAIN medicines often cause unexpected side effects. Medicines are desired to localize at the target organs, but in some cases they reach other organs, causing harm to patients. Therefore, we need to recognize *in vivo* dynamics and kinetics. In order to analyze this, radioisotope-tagged drugs such as ^{14}C or ^{18}F [1], [2] are commonly used as tracers. However, radioisotope-tagging methods have some disadvantages; radiation can cause damage to the sample, be harmful to researchers, and is financially costly. Despite the drawbacks of the radioisotope method, it is routinely used as the only available technique. We have applied quantum dots (QDs) to trace medicine instead of radioisotope method.

Manuscript received May 30, 2006; revised August 8, 2006. This work was supported in part by the Ministry of Health, Labor and Welfare of Japan under Medical Techniques Promotion Research Grant H14-nano-004 to K. Yamamoto and in part by the Japan Foundation of Cardiovascular Research under a Bioimaging Grant to A. Hoshino. *Asterisk indicates corresponding author.*

N. Manabe and T. Goto are with the International Clinical Research Center, Research Institute, International Medical Center of Japan, Tokyo 162-8655, Japan.

A. Hoshino is with the International Clinical Research Center, Research Institute, International Medical Center of Japan, Tokyo 162-8655, Japan. He is also with the Hospital Pharmacy, Tokyo Medical and Dental University Graduate School, Tokyo 113-8519, Japan.

Y. Liang and N. Kato are with the Department of Gene Diagnostics and Therapeutics, Research Institute, International Medical Center of Japan, Tokyo 162-8655, Japan.

*K. Yamamoto is with the International Clinical Research Center, Research Institute, International Medical Center of Japan, Tokyo 162-8655, Japan. He is also with the Hospital Pharmacy, Tokyo Medical and Dental University Graduate School, Tokyo 113-8519, Japan (e-mail: backen@ri.imcj.go.jp).

Digital Object Identifier 10.1109/TNB.2006.886569

QDs are semiconductor particles a few nanometers in size, and have been currently used in biomedical studies due to their brighter fluorescence [3]–[11]. We attached a medicine to QDs and observed whether they retain a medicinal effect *in vivo*. First, we conjugated QDs with an anti-hypertension medicine, captopril [12], [13], and measured effect of QD-conjugated captopril (QD-cap) *in vitro*. Furthermore, we administered them to the spontaneously hypertensive rat and assessed the effect of QD-medicine *in vivo*.

II. Materials and Methods

A. Synthesis and Purification of QD-Cap

QDs were enfolded into the micelle of *n*-trioctylphosphine oxide (QD-TOPO). QD-cap was produced by replacing QD-TOPO by the captopril as follows; Captopril (Sankyo Co., Ltd; Japan) dissolved in ethanol was added dropwise into the QD-TOPO solution in tetrahydrofuran (Wako Pure Chemical Industries, Ltd., Japan) and then the mixture was heated to 85 °C, and refluxed for 12 h. After the reaction, NaOH solution (pH10) was added, and the mixture was heated at 90 °C to removed the tetrahydrofuran by evaporation. The obtained aqueous solution with QD-cap was then purified and concentrated with an ultrafiltration membrane (Millipore Corp., MA, Microcon YM-3). Purification was performed with a gel filtration column (GE Healthcare Bio-Sciences Corp., NJ, MicroSpin G-25 Columns). Images of the samples were taken using a digital camera D1H (Nikon Corp., Japan) with 1/25 s exposure excited by a 365-nm wavelength (UV-A).

B. High-Performance Liquid Chromatography (HPLC)

The products in the aqueous solution were analyzed with an HPLC (Waters Corp., MA, 600E Multisolvent Delivery System, Waters Corp. 2487 Dual λ Absorbance Detector, and Waters Corp. 2475 Muiti λ Fluorescence Detector) to identify and quantify the QD-cap. A QD sample was applied to a gel permeation column (GE Healthcare Bio-Sciences Corp., MAbTrap Kit) and 20% methanol was used as a mobile phase (0.04 mL/min). The UV detector monitored the absorbance at 230 nm.

C. Measurement of ACE Inhibitory Activity

Inhibitory activity of angiotensin I-converting enzyme (ACE) was established by the method of Cushman and Cheung with some modification [14], a method based on the characteristic of ACE liberating hippuric acid from hippuryl-His-Leu. The 50 μL of ACE (Sigma-Aldrich Corp., MO) in borate buffer [22.5 mM Na_2B_4O-110 mM H_3BO_3] (pH8.3) (6 mU) was mixed with 50 μL of the sample of the same concentration of captopril (distilled water as a blanc), and added 50 μL of 1.2 M NaCl and then the mixture was preincubated at 37 °C

for 3 min. The reaction was initiated by adding 50 μL of borate buffer [pH8.3] containing 10 mM hippuryl-His-Leu (Peptide Institute Inc., Japan). The mixture was incubated at 37 °C for 30 min. The reaction was stopped by the addition of 200 μL of 1 M HCl. The hyppuric acid liberated from the ACE reaction was extracted with 1 mL of ethyl acetate, and the solvent was removed by vacuum evaporation. The content was dissolved by addition of 1 mL of distilled water and its UV spectra density at 228 nm was measured. The percentage of inhibition is calculated as follows:

$$\% \text{ Inhibition} = \frac{(B - A)}{(B - C)} \times 100$$

where A is the UV spectra density in the presence of a sample, B the UV spectra density in the presence of distilled water instead of a sample, and C the UV spectra density in the presence of a sample and 1 M HCl.

D. Stroke-Prone Spontaneously Hypertensive Rats (SHRSP)

SHRSP (12 weeks, male) (275±20 g) were purchased from Japan SLC Inc. The SHRSP were anesthetized with diethyl ether and the samples were injected into the carotid artery (5 mg/kg). Systolic blood pressures (SBP) were measured using the tail-cuff method 0, 15, 30, and 60 min after the injection, respectively ($N = 3$).

E. Concentration of QD-Cap in Plasma and the Separation of the Cells and Organs

The SHRSP were anesthetized and the QD-cap was injected into the carotid artery (7 mg/kg). The SHRSP were sacrificed 0.5, 1, 2, 4, 8, 16, 24, 48, 72, and 96 h after the injection and the peripheral blood was collected using 200 U of heparin in a tube. The blood was centrifuged at 10 000 g for 5 min at room temperature to let it form a distinct layer at the plasma–blood cell interface. The plasma layer was separated from the blood cell layer. The fluorescent intensity at 630 nm of QD-cap in plasma was measured by spectrofluorometer (JASCO Corp., Japan, FP-6500) with the different concentration of QD-cap. QD-cap concentrations of plasma obtained from SHRSP were calculated based on the fluorescent intensity.

The collected brain, kidney, liver, lung, and spleen were immediately washed twice by PBS to remove the retained erythrocytes. Then each organ was incubated with 4% paraformaldehyde for 2 h at room temperature. After soaking, the organs were washed and incubated three times with 100% ethanol at 4 °C for 3 h. After embedded into paraffin, the section was sliced into pieces to 10 μm thickness, and they were affixed to a slide glass. Images were acquired with a digital camera D1X (Nikon Corp.) on a fluorescent microscope IX-81 (Olympus Corp., Japan) using a WUV mirror unit to adjust the excitation wavelength to 330–385 nm and oil immersion objective lens. Fluorescence intensity of QDs was quantitatively measured making use of an imaging analyzer (Adobe Systems Inc., CA, Photoshop ver. 8.0.1).

III. Results

A. Synthesis of QD-Conjugated Captotril

We synthesized CdSe/ZnS-core/shell-typed QDs by the hot soap method with tri-n-octyl phosphine oxide (TOPO) as reported before [15]–[17]. We replaced the TOPO on the surface of QD with captopril by a thiol-exchange reaction. Captopril has a sulfhydryl group and can be directly coordinated on the surface of QDs [Fig. 1(a) and (b)]. We purified the newly synthesized QD-cap with an ultrafiltration membrane and a gel filtration. Purification of the QD-cap was confirmed by HPLC with absorbance which is specific to captopril (230 nm). The retention time of the QD-cap was observed in 22–24 min, whereas unconjugated captopril was observed near 33 min [Fig. 1(c)]. The peak of unconjuagted QDs appeared later. Furthermore, no peak near 33 min was observed in the purified QD-cap (arrowhead), indicating the unreacted captopril had been removed. We confirmed the collection of the QD-cap with their intrinsic fluorescence of 630 nm (data not shown).

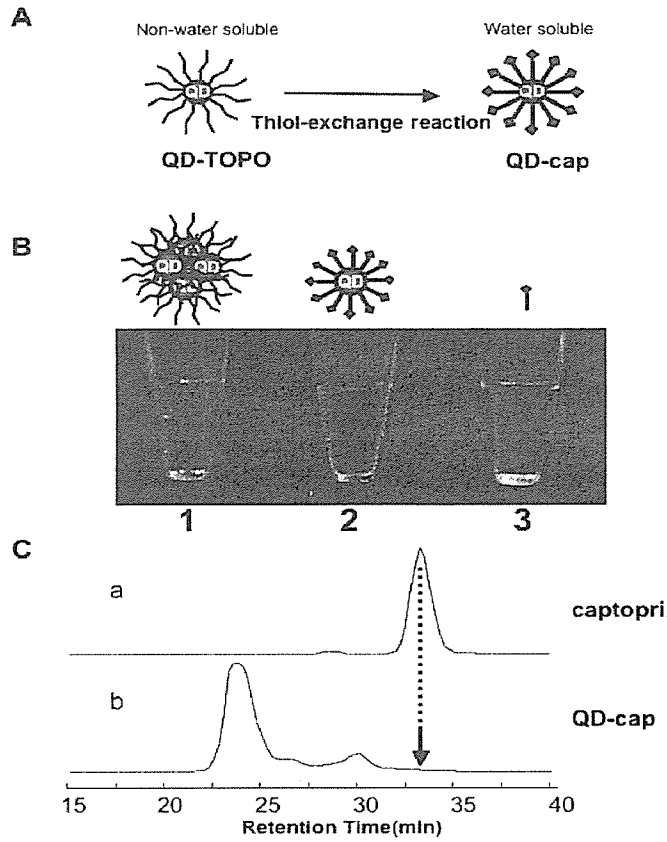

Fig. 1. (A) QD-cap was synthesized using thiol-exchange reactions. (B) The image of the samples in water was taken using a digital camera D1H (Nikon Corp.) with 1/25 s exposure excited by a 365-nm wavelength. (1) QD-TOPO insoluble as seeing aggregation. (2) QD-cap solution. (3) Captopril only. (C) QD-cap in aqueous solution was analyzed with an HPLC. The UV detector monitored the absorbance at 230 nm. (a) Captopril (b) QD-cap.

B. ACE Inhibitory Activity of QD-Cap In Vitro

Captopril acts to inhibit ACE, which converts hypertensive precursor peptides to their active form [12], [13]. Therefore, we confirmed whether QD-cap has maintained the activity to block ACE. The blocking activity was measured *in vitro*. QD-cap inhibited ACE as efficiently as captopril (Fig. 2). In contrast, thioglycerol coated QDs (QD-OHs) did not inhibit any ACE activity. QD-cap retained the inhibitory activity of ACE at the level of unconjugated captopril *in vitro*. This result suggests that we synthesized the functional nanoparticle of QD and captopril without losing the fluorescence activity and anti-hypertensive

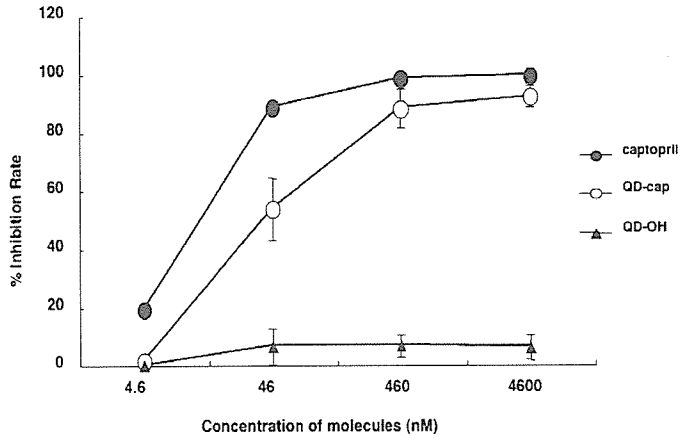

Fig. 2. Inhibition activity of angiotensin I -converting enzyme (ACE) by QD-cap was measured by the method of Cushman and Cheung with some modification. The y axis indicates the percent inhibition. The data presented is the mean value and standard deviation of triplicate samples. Captopril (•); QD-cap (○); QD-OH (▲).

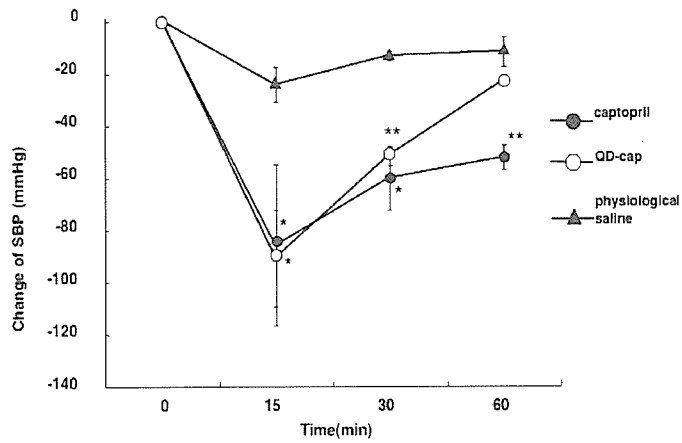

Fig. 3. QD-cap (5 mg/kg) was injected into the SHRSP via carotid artery. Systolic blood pressures were measured using tail-cuff method at indicated time. ($N = 3$). Each data presents the mean value and standard deviation of triplicate samples. Captopril (•), physiological saline (▲), QD-cap (○), $*, p < 0.05$. $**, p < 0.01$.

effect. By taking advantage of the fluorescence of QDs, the mobility of QD-medicine can be traced inside the body.

C. *QD-Cap Exerts Anti-hypertensive Effect in Vivo*

The fact that QD-cap showed ACE inhibition *in vitro* prompted us to assess the anti-hypertensive effect *in vivo*. The samples were injected into the SHRSP and the systolic blood pressure was measured using the tail-cuff method. The blood pressure was decreased after the administration of the QD-cap as well as the administration of captopril up to at least 30 min to the same extent (Fig. 3). Contrary to our expectation, the blood pressure of QD-cap administered rats relapsed to the original level 60 min after the injection, whereas the anti-hypertensive effect of the unconjugated captopril was still maintained. We first expected that QD-cap would exert more beneficial effects than captopril only. However, in some cases QD-cap was less active than captopril only. The surface of the QD-cap was covered with the hundreds of captopril molecules. So we assumed that captopril molecules all together are captured to blood proteins such as albumin and metabolize at the same time.

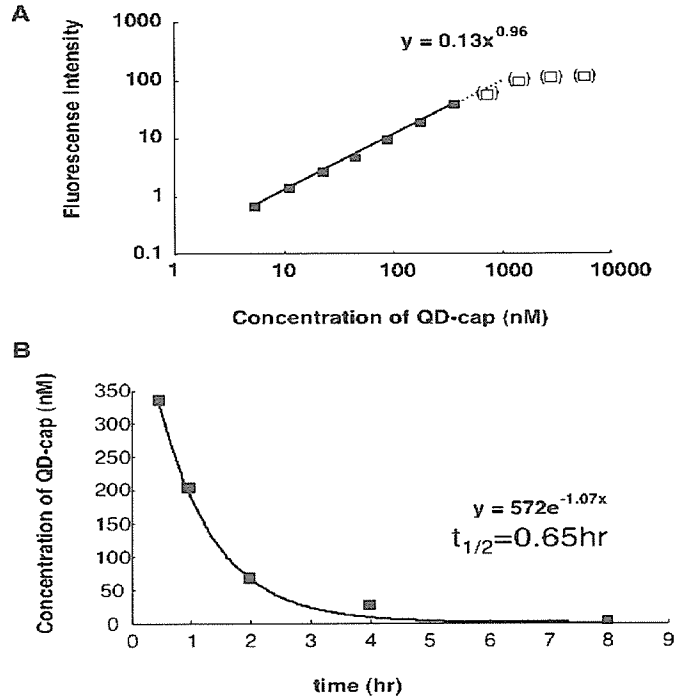

Fig. 4. (A) Fluorescence intensity and the concentration of QD-cap. The relative fluorescence intensity of QD-cap were plotted against the concentration diluted by the plasma obtained from SHRSP. Fluorescent intensity at 630 nm of QD-cap in plasma was measured by spectrofluorometer (JASCO FP-6500) with the different concentration of the QD-cap. We plotted the relative fluorescent intensity of the QD-cap against the concentration diluted by the QD-cap obtained from SHRSP. (B) Fluorescent intensity at 630 nm of QD-cap in plasma was measured by spectrofluorometer. The SHRSP were sacrificed at the indicated time after injection (7 mg/kg) and the plasma was collected. QD-cap concentrations of plasma obtained from SHRSP were calculated on the basis of Table I.

D. *QD-Fluorescence Displays QD-Cap Concentration in Blood*

The fluorescence emitted from QD-cap can be measured easily. For the measurement of the concentration of the QD-cap in the plasma, we made the standard curve of the concentration of the QD-cap versus the fluorescence intensity. The samples of the QD-cap in the range from 5.6 nM to 5750 nM dissolved in the plasma were prepared for the measurement of the fluorescence intensity. We plotted the concentration of the QD-cap against the fluorescence intensity, and the curve showed linearity in the range of 5.6 to 359.4 nM [Fig. 4(a)]. Then we analyzed the concentration of the QD-cap chronologically in the blood. The plasma was obtained from the SHRSP, and fluorescence intensity was measured (Table I). The concentration of QD-cap decreased exponentially and the half-life was calculated as 0.65 h [Fig. 4(b)]. This result is consistent with the report that the half-life of the captopril is 0.43 h (personal communication with Sankyo Co. Ltd.).

These results suggested that the fluorescence intensity of the QD-cap can be utilized as a convenient indicator *in vivo*.

E. *QD-Fluorescence Reveals Distribution of QD-Cap In Vivo*

Since measurement of fluorescence intensity of the QD-cap revealed the kinetics of the QD-cap, we then tried to assess the distribution of QDs in the brain, liver, kidney, lung, and spleen chronologically. The organs were collected from the SHRSP at the indicated times after the injection, and were sliced to the serial tissue sections. The estimated concentration of QD-cap in

TABLE I
TIME COURSE OF FLUORESCENCE INTENSITY AND THE CONCENTRATION OF QD-CAP IN BLOOD

Time (hr)	Fluorescence Intensity	QD-cap concentration (nM)
0	1.39	nt
0.5	35.60	329.6
1	22.60	200.1
2	8.77	66.5
4	4.46	26.6
8	1.82	3.4
16	0.61	nt
24	0.76	nt
48	0.83	nt
72	0.76	nt
96	0.89	nt

nt stands for not tested.

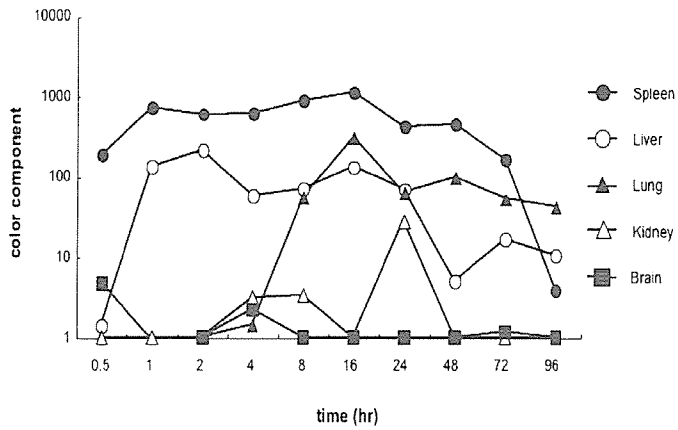

Fig. 5. The distribution of QD-cap was measured. The rats were sacrificed at the indicated time and the QD-cap in organ were analyzed. Crypsections were captured with a digital camera on a fluorescent microscope and color component of QDs was quantitatively measured making use of an imaging analyzer (Adobe Photoshop). Spleen (●); liver (○); lung (▲); kidney (△); brain (■).

each organ was analyzed chronologically based on the imaging analyzer (see Section II). The distribution of QD was significantly different from organ to organ (Fig. 5). In the spleen, the fluorescence intensity rapidly rose and stayed at that level for a long time; it reached a peak in an hour, and took 48 h to return to the original level. In the case of the liver, the intensity reached the peak in 2 h and decreased gradually in 96 h. In the lung the intensity rose slowly, reaching the peak at 16 h after the injection and then decreased slowly in 96 h. In contrast, we detected only a low level of fluorescence in the brain and in the kidney. Thus, QD-cap, as captopri, can be distributed among the organs and blood.

IV. DISCUSSIONS

In this study, we synthesized the functional nanocomposite particles of QD and captopril without losing the fluorescence activity and anti-hypertensive effect. The fluorescence of QDs revealed the dynamics and kinetics of QD-medicine inside the body. In order to trace the kinetics and dynamics of a medicine, a lot of researchers have used radioisotopes in the *in vivo* studies. With our novel method, as shown in Figs. 4 and 5, the blood concentration of a medicine can be measured. Moreover, the localization of the medicine inside the organs can be detected. In addition, measurement of fluorescence requires less time than radioisotope methods. Gao *et al.* [18] and Ballou *et al.* [19] have reported that the fluorescence generated from QD inside the body of the living mouse was detected by using a detection system of QD. With the development of the *in vivo* imaging systems, QD-tagged medicine techniques may contribute not only to analyze the mechanism of the side effects but to produce new medicines in the future.

We expected that QD-cap could exert stronger effects than unconjugated captopril. However, QD-captopril activity was weaker than that of unconjugated captopril. We interpret that the hundreds of captopril molecules concentrated on the surface of the QD-cap are easily captured and metabolized by cells such as phagocytes and endothelium. All captopril molecules on the surface of QD lose their activity if one of the captopril on QD-cap was captured. In contrast, QD-cap induced no change to the properties such as the beneficial effect and lifetime. The rapid decrease of the concentration of the QD-cap in the blood vessels an hour after the administration (shown in Fig. 4) is consistent with the observation that the decreased blood pressure rapidly recovered within an hour (shown in Fig. 3).

We have succeeded in the localization of QDs in the cellular organelles such as nuclei, mitochondria, and lysosomes of the living cells [20]. We can also conjugate the surface of the QD with more than two different compounds [21]. Further development of these technologies in the near future will enable QD-tagged medicine to be commonly used as an effective drug delivery system into the specific organs by using the targeted peptides [22].

We have previously reported that several factors such as QD concentration [23], incubation time [24], and surface-processing [21] were concerned with the cytotoxicity of QD. In this paper, we examined *in vivo* study with QD-medicine of CdSe/ZnS. Derfus *et al.* [25] reported that core-shell typed QD irradiated with ultraviolet more than 8 h showed the cytotoxicity by the leaked Cd^{2+} ion, but no sign of cytotoxicity in

case of 1 h exposure. We also found no sign of cytotoxicity under the condition of our *in vitro* experiments. In addition, no body weight loss was found after a wide range of doses of the QD-cap *in vivo*. The lifespan of QD treated animals showed no difference from that of untreated ones. This result is consistent with the report of Derfus *et al.* QD made from cadmium materials could generate toxic cadmium ions that might exhibit the cytotoxicity in some unexpected cases. Warner *et al.* reported the method of the production of silicon dots [26]. Further study will make possible clinical applications of QDs made from materials more suitable for the safety such as silicon.

ACKNOWLEDGMENT

The authors would like to thank Dr. K. Omata, Mr. K. Ito, Mr. S. Ohhara, and Mr. K. Arakawa of the International Clinical Research Center, Research Institute, IMCJ, for their valuable assistance; and Dr. H. Yoshikura (Ministry of Health Labour and Welfare, Japan) and Dr. R. Tilley (Victoria University of Wellington, New Zealand) for their helpful advice. The authors are also grateful to Sankyo Co. Ltd. (Tokyo, Japan) for kindly providing captopril.

REFERENCES

[1] O. Chiewitz and G. Hevesy, "Radioactive indicators in the study of phosphorus metabolism in rats," *Nature*, vol. 136, pp. 754–755, 1935.
[2] N. S. Mason and C. A. Mathis, "Positron emission tomography radiochemistry," *Neuroimag. Clin. N. Amer.*, vol. 13, pp. 671–687, 2003.
[3] T. C. Harman, P. J. Taylor, M. P. Walsh, and B. E. LaForge, "Quantum dot superlattice thermoelectric materials and devices," *Science*, vol. 297, pp. 2229–2232, 2002.
[4] X. Wu, H. Liu, J. Liu, K. N. Haley, J. A. Treadway, J. P. Larson, N. Ge, F. Peale, and M. P. Bruchez, "Immunofluorescent labeling of cancer marker Her2 and other cellular targets with semiconductor quantum dots," *Nature Biotechnol.*, vol. 21, pp. 41–46, 2003.
[5] B. Dubertret, P. Skourides, D. J. Norris, V. Noireaux, A. H. Brivanlou, and A. Libchaber, "In vivo imaging of quantum dots encapsulated in phospholipid micelles," *Science*, vol. 298, pp. 1759–1762, 2002.
[6] W. C. W. Chan and S. Nie, "Quantum dot bioconjugates for ultrasensitive nonisotopic detection," *Science*, vol. 281, pp. 2016–2018, 1998.
[7] M. Bruchez, Jr, M. Moronne, P. Gin, S. Weiss, and A. P. Alivistos, "Semiconductor nanocrystals as fluorescent biological labels," *Science*, vol. 281, pp. 2013–2016, 1998.
[8] D. Ishii, K. Kinbara, Y. Ishida, N. Ishii, M. Okochi, M. Yohda, and T. Aida, "Chaperonin-mediated stabilization and atp-triggered release of semiconductor nanoparticles," *Nature*, vol. 423, pp. 628–632, 2003.
[9] J. K. Jaiswal, H. Mattoussi, J. M. Mauro, and S. M. Simon, "Long-term multiple color imaging of live cells using quantum dot bioconjugates," *Nature Biotechnol.*, vol. 21, pp. 47–51, 2003.
[10] D. R. Larson, W. R. Zipfel, R. M. Williams, S. W. Clark, M. P. Bruchez, F. W. Wise, and W. W. Webb, "Water-soluble quantum dots for multiphoton fluorescence imaging in vivo," *Science*, vol. 300, pp. 1434–1436, 2003.
[11] G. T. Shubeita, S. K. Sekatskii, G. Dietler, I. Potapova, A. Mews, and T. Basche, "Scanning near-field optical microscopy using semiconductor nanocrystals as a local fluorescence and fluorescence resonance energy transfer source," *J. Microsc.*, vol. 210, pp. 274–278, 2003.
[12] B. Rubin, R. J. Laffan, D. G. Kotler, E. H. O'Keefe, D. A. Demaio, and M. E. Goldberg, "SQ 14225 (D-3 mercapto-2-methylpropanoyl-L-proline), a novel orally active inhibitor of angiotensin I-converting enzyme," *J. Pharmacol. Exp. Ther.*, vol. 204, pp. 271–280, 1978.
[13] R. J. Laffan, M. E. Goldberg, J. P. High, T. R. Schaeffer, M. H. Waugh, and B. Rubin, "Antihypertensive activity in rats for sq 14225, an orally active inhibitor of angiotensin I-converting enzyme," *J. Parmacol. Exp. Ther.*, vol. 204, pp. 281–288, 1978.
[14] D. W. Cushman and H. S. Cheung, "Spectrophotometric assay and properties of the angiotensin-converting enzyme of rabbit lung," *Biochem. Pharmacol.*, vol. 20, pp. 1637–1648, 1971.
[15] B. O. Dabbousi, J. Rodriguez-Viejo, F. V. Mikulec, J. R. Heine, H. Mattoussi, R. Ober, K. F. Jensen, and M. G. Bawendi, "(CdSe)ZnS core-shell quantum dots: Synthesis and characterization of a size series of highly luminescent nanocrystallites," *J. Phys. Chem. B*, vol. 101, pp. 9463–9475, 1997.
[16] M. A. Hines and P. Guyot-Sionnest, "Synthesis and characterization of strongly luminescing ZnS-capped CdSe nanocrystals," *J. Phys. Chem.*, vol. 100, pp. 468–471, 1996.
[17] C. B. Murray, D. J. Norris, and M. G. Bawendi, "Synthesis and characterization of nearly monodisperse CdE (E = S, Se, Te) semiconductor nanocrystallites," *J. Amer. Chem. Soc.*, vol. 115, pp. 8706–8715, 1993.
[18] X. Gao, Y. Cui, R. M. Levenson, L. W. Chung, and S. Nie, "In vivo cancer targeting and imaging with semiconductor quantum dots," *Nature Biotechnol.*, vol. 22, pp. 969–976, 2004.
[19] B. Ballou, B. C. Lagerholm, L. A. Ernst, M. P. Bruchez, and A. S. Waggoner, "Noninvasive imaging of quantum dots in mice," *Bioconjugate Chem.*, vol. 15, pp. 79–86, 2004.
[20] A. Hoshino, K. Fujioka, N. Manabe, S. Yamaya, Y. Goto, M. Yasuhara, and K. Yamamoto, "Simultaneous multicolor detection system of the single-molecular microbial antigen with total internal reflection fluorescence microscopy," *Microbiol. Immunol.*, vol. 49, pp. 461–470, 2005.
[21] A. Hoshino, K. Fujioka, T. Oku, M. Suga, Y. F. Sasaki, T. Ohta, M. Yasuhara, K. Suzuki, and K. Yamamoto, "Physicochemical properties and cellular toxicity of nanocrystal quantum dots depend on their surface modification," *Nano Lett.*, vol. 4, pp. 2163–2169, 2004.
[22] M. E. Akerman, W. C. Chan, P. Laakkonen, S. N. Bhatia, and E. Ruoslahti, "Nanocrystal targeting in vivo," *Proc. Nat. Acad. Sci. USA*, vol. 99, pp. 12617–12621, 2002.
[23] A. Shiohara, A. Hoshino, K. Hanaki, K. Suzuki, and K. Yamamoto, "On the cyto-toxicity caused by quantum dots," *Microbiol. Immunol.*, vol. 48, pp. 669–675, 2004.
[24] A. Hoshino, K. Hanaki, K. Suzuki, and K. Yamamoto, "Applications of T-lymphoma labeled with fluorescent quantum dots to cell tracing markers in mouse body," *Biochem. Biophys. Res. Commun.*, vol. 314, pp. 46–53, 2004.
[25] A. M. Derfus, W. C. W. Chan, and S. N. Bhatia, "Probing the cytotoxicity of semiconductor quantum dots," *Nano Lett.*, vol. 4, pp. 11–18, 2004.
[26] J. H. Warner, A. Hoshino, K. Yamamoto, and R. D. Tilley, "Water-soluble photoluminescent silicon quantum dots," *Angew. Chem. Int. Ed. Engl.*, vol. 44, pp. 4550–4554, 2005.

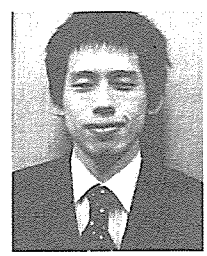

Noriyoshi Manabe was born in Japan on February 1, 1980. He received the M.S. degree in pharmacy from the Kyoritsu University of Pharmacy Graduate School, Tokyo, Japan, in 2004.

Since 2004, he has been a Researcher with the International Clinical Research Center, Research Institute, International Medical Center of Japan, Tokyo. In university, he studied specially about medicine and transcription factors. His research interests include bioimaging and drug delivery systems using quantum dots.

Mr. Manabe is a Registered Pharmacist.

Akiyoshi Hoshino, photograph and biography not available at the time of publication.

Yi-qiang Liang, photograph and biography not available at the time of publication.

Tomomasa Goto, photograph and biography not available at the time of publication.

Norihiro Kato, photograph and biography not available at the time of publication.

Kenji Yamamoto, photograph and biography not available at the time of publication.

Visualizing Vitreous Using Quantum Dots as Imaging Agents

Satoru Yamamoto, Noriyoshi Manabe, Kouki Fujioka, Akiyoshi Hoshino, and Kenji Yamamoto*

Abstract—**Vitreous is transparent tissue located between the lens and the retina of the eye, thus, difficult to look at by even ophthalmological microscope. But vitreous is connected with some sight-threatening eye diseases, for example, retinal detachment, macular hole, epi-retinal membrane, and so forth. Quantum dots (QDs) have been applied to a wide range of biological studies by taking advantage of their fluorescence properties. We established a novel technique of aqueous colloidal QD (ACQD) as a vitreous lesion detector. When compared with some conventional dyes used for clinical situation, i.e. fluorescein, indocyanine green, and triamcinolone acetonide, ACQD exerted a higher performance to detect a Weiss Ring. Furthermore ACQD is also effective to perform vitrectomy, an eye surgery to cut and eliminate vitreous. Some functional structures in vitreous are detected clearly when ACQD was injected into an enucleated porcine eye. We demonstrated that ACQD enabled any ophthalmic surgeon to perform vitrectomy reliably, easily, and more safely. Taken together, the ACQD-oriented vitreous staining system will promote ophthalmological science, and it will raise the cure rate of eye diseases.**

Index Terms—**Aqueous colloidal quantum dot, vitrectomy, vitreous imaging reagents.**

I. Introduction

ALTHOUGH IT IS very important to understand the general structure and substructure of the eye [1], the lack of adequate methods to image transparent vitreous makes it very difficult to fully understand vitreous normal structure, function, and how these change during aging and disease [2], [3], because the vitreous is jellylike tissue that is filled with transparent collagen and hyaluronate. Thus, it is required to develop a new vitreous visualizing method for ophthalmologists to observe the pathology of vitreous [4]–[8]. Here we demonstrate that a novel visualizing tool with aqueous colloidal quantum dots (ACQDs) enables us to image and observe the transparent vitreous lesion clearly.[1]

It has been shown recently that many eye diseases are connected with pathologic and/or physiological changes of the vitreous. Liquefaction of vitreous through aging may be involved in retinal tear which may lead to retinal detachment, and eventually to lack of light perception. The epiretinal membrane is thought to be connected with posterior vitreous denature after liquefaction. In addition, it caused some complicated diseases such as proliferative vitreoretinopathy, macular hole, retinopathy of prematurity, and proliferative diabetic vitreoretinopathy. As for vitreous around the posterior pole of the eye, optical coherence tomography (OCT) was invented (particularly ultrahigh-resolution OCT [9]) and solved the question of macular hole formation [10], [11]. But there is no adequate method to observe transparent vitreous in daily clinical situations. In addition, it is difficult to observe the vitreous in the case of vitreous surgery (called vitrectomy). As a result, the inability to image vitreous adequately may induce unavoidable errors in the operation such as damaged retina.

Several organic dyes including fluorescein and indocyanine green have been used as imaging agents for retinal and choroidal vessels [12], but they have difficulties for diagnosis for vitreous cavity. A turbid corticosteroid, triamcinolone acetonide (TA), is also used as an imaging reagent in some special cases; improvement of diabetic macular edema or for vitrectomy, but some side effects have been reported such as the elevation of intraocular pressure, acceleration of cataract, and endophthalmitis [13]–[15]. Therefore, it is important to develop new vitreous visualizing materials and a method not only for ophthalmologists to observe the pathology of vitreous but also to treat vitreous-related diseases.

II. Materials and Methods

A. Materials

Some porcine eyes (approximately 6 months old) were purchased from Tokyo Metropolitan Slaughterhouse (Tokyo, Japan) as a virtual human eye to perform vitrectomy training for ophthalmological residents.

Some aged porcine eyes (approximately 8 years old) were provided from Tokushima A. F. F. Technology Support Center (Tokushima, Japan) as aged vitreous lesion models.

B. Synthesis and Purification of ACQDs

ACQDs were synthesized by replacing QD-TOPO with the aqueous dipeptide (1-[(2S)-3-mercapto-2-methylpropionyl]-L-

Manuscript received August 28, 2006; revised December 6, 2006. This work was supported in part by the Ministry of Health, Labor and Welfare of Japan under Medical Techniques Promotion Research Grant H14-nano-004 (K. Yamamoto), and in part by a bioimaging grant from Japan Foundation of Cardiovascular Research (A. Hoshino).

S. Yamamoto is with the Department of Ophthalmology, Yokohama Sakae Kyousai Hospital, Yokohama, Japan.

N. Manabe and K. Fujioka are with the Research Institute, International Medical Center of Japan, Shinjuku-ku, Tokyo 162-8655 Japan.

A. Hoshino is with the Research Institute, International Medical Center of Japan, Tokyo 162-8655, Japan and also with the Department of Pharmacokinetics and Pharmacodynamics, Tokyo Medical and Dental University Graduate School, Tokyo 113-8519, Japan.

*K. Yamamoto is with the Research Institute, International Medical Center of Japan, Tokyo 162-8655, Japan and also with the Department of Pharmacokinetics and Pharmacodynamics, Tokyo Medical and Dental University Graduate School, Tokyo 113-8519, Japan (e-mail: backen@ri.imcj.go.jp).

Digital Object Identifier 10.1109/TNB.2007.891883

[1]Supplemental movies: This information is available free of charge via the Internet at http://www.geocities.jp/backenlab/.

proline) as follows: aqueous dipeptide solution in ethanol was dripped into the QD-TOPO solution in tetrahydrofuran (Wako Pure Chemical Industries, Ltd.; Osaka, Japan) and then the mixture was warmed up to 85 °C, and refluxed for 12 h. After the reaction, NaOH solution (pH10) was added and the mixture was heated at 90 °C to remove the contained tetrahydrofuran by evaporation. The obtained ACQDs solution was then purified and concentrated with an ultrafiltration membrane (Amicon Ultra-4, Millipore Corporation, Billerica, MA). The final purification was performed with a gel filtration column (MicroSpin G-25 Columns, Amersham Bioscience, San Francisco, CA).

C. *Vitrectomy*

A standard 3-port pars plana vitrectomy was performed on a porcine eye (6 months old) mounted in a human head model using a 20-gauge vitreous cutter and a hand-held light pipe. Sclerotomies were placed 3.5 mm posterior to the corneal limbus in the superotemporal, superonasal and inferotemporal quadrants. The infusion cannula was sutured in the inferotemporal sclerotomy site. The 20-gauge hand-held light pipe was inserted first into the vitreous cavity, then the vitreous cutter was inserted. Finally, the vitreous was cut and eliminated by vitreous cutter. The porcine eye stained with QDs will be an excellent vitrectomy training device as a virtual human eye for ophthalmology residents.

III. Results

A. *Detection of Weiss Ring With ACQDs*

We evaluated whether ACQDs are effective to detect the Weiss ring (WR). The WR is a ring-shaped structure of posterior vitreous in the vitreous cavity, formerly attached with the optic nerve disc (Fig. 1). Aging accelerates the liquefaction of the vitreous and the posterior vitreous detachment (PVD) from the retina. But posterior vitreous attaches with the optic nerve disc strongly, then the final step of posterior vitreous detachment forms the WR structure. Therefore, in clinical situations, the eye with WR is regarded as the eye with PVD. It is very important to diagnose PVD. If posterior vitreous attaches with the retina, blood vessels of the retina enter directly into the vitreous. Then, proliferative eye diseases deteriorate rapidly. However, it is difficult to detect the PVD in clinical situations. Since the white light used for inspection reflects from the retina, the contrast of the retina and WR is indistinguishable.

To visualize the transparent vitreous, we injected the ACQDs (red emitting 640 nm) into the vitreous cavity of an enucleated aged and a young porcine eye with a 27-gauge needle via pars plana of the ciliary body (Fig. 2). In order to examine the effect of ACQDs, the efficiency of ACQDs was compared with that of a conventional dye TA. Just after the injection of ACQDs, they dispersed into the vitreous cavity (see supplementary movie S1). The fluorescence reflection from ACQDs made it possible to observe the structure in the posterior side of the vitreous cavity. The striking contrast enables us to observe vitreous structures by a slit lamp microscopy without any difficulty [Fig. 2(a), 2(b)]. Consequently the details of the status of vitreous are detected easily because ACQDs can be excited by a white lump which is commonly used as a light source. In contrast, TA fails to visualize the subtle vitreous structures because it is turbid in vitreous [Fig. 2(c)]. As a result, ACQDs enable us to detect details of the status of the vitreous at striking contrast.

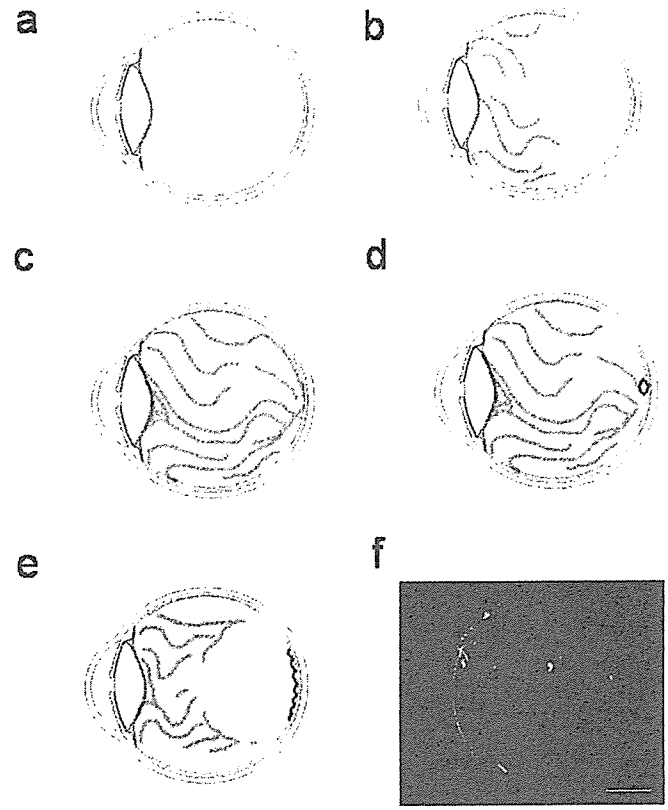

Fig. 1. Age-related change of vitreous lesion. (a) The vitreous of the neonatal eye. The vitreous cavity is uniform and the fiber of the vitreous gel (collagen and hyarulonate with water) exists in the radial pattern. (b) The vitreous of the young eye. The tractus was formed in former vitreous whereas the structure of the latter cavity still remained. (c) The vitreous of the aged eye. The tractus formation was expanded to all the vitreous cavity. (d) The PVD formed eye. Liquefaction of the vitreous gel started. The red circle indicates the WR. (e) The structure of the PVD-developed eye. In some cases, posterior vitreous gel located in the latter cavity. (f) Distribution of ACQDs in the vitreous. ACQD solution (200 μL) was injected into the vitreous cavity and then the whole eye was frozen. The cryosection of the whole eyeball was observed on a fluorescent microscopy equipped with a cooled CCD camera. The illustration of the eye structure was superimposed onto the photo image. The bar indicates 10 mm.

B. *ACQDs With a Vitreous Staining Device for Vitrectomy*

This result encouraged us to use ACQDs as an imaging agent for vitrectomy. There are few imaging agents used for vitrectomy, and it is quite difficult to remove all vitreous lesions without making new iatrogenic lesions. To demonstrate the efficiency of ACQDs, a vitrectomy on the porcine eye was performed under a surgical microscopy and compared with these conventional organic probes. First we injected the organic fluorescent probes and evaluated them. Fluorescein, which emits yellow-green fluorescence, is too bright in the vitreous to discern between the optical reflection from the retina and vitreous lesion [Fig. 3(a)]. Another organic dye, indocyanine green, which is used for diagnosis of age-related macular degeneration, is an infrared fluorescent probe and not suitable for dye for vitrectomy [Fig. 3(b)]. In contrast, the ACQD-probe

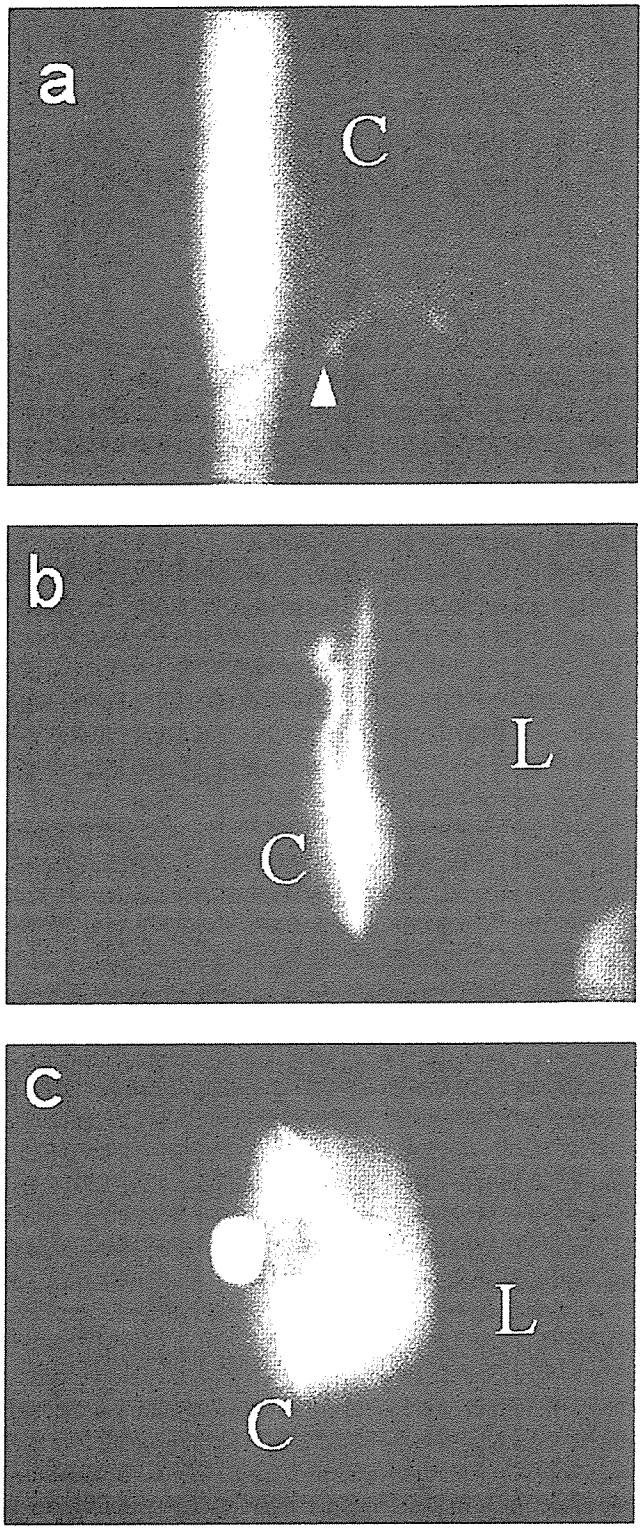

Fig. 2. ACQDs enable us to visualize the structure in vitreous at striking contrast. (a) The vitreous of the aged eye was observed with a slit lamp microscopy using ACQDs. The arrowhead indicates the WR. (b) The anterior view of the young eye with direct illumination showed the iatrogenic cavity in vitreous located just behind the lens. Fluorescence emitted from ACQD reflected the structures of vitreous and enabled us to observe easily. (c) The injection of triamcinolone acetonide (TA) identified the structure of the vitreous poorly because the particle of TA was very big and turbid. C: iatrogenic cavity; L: lens.

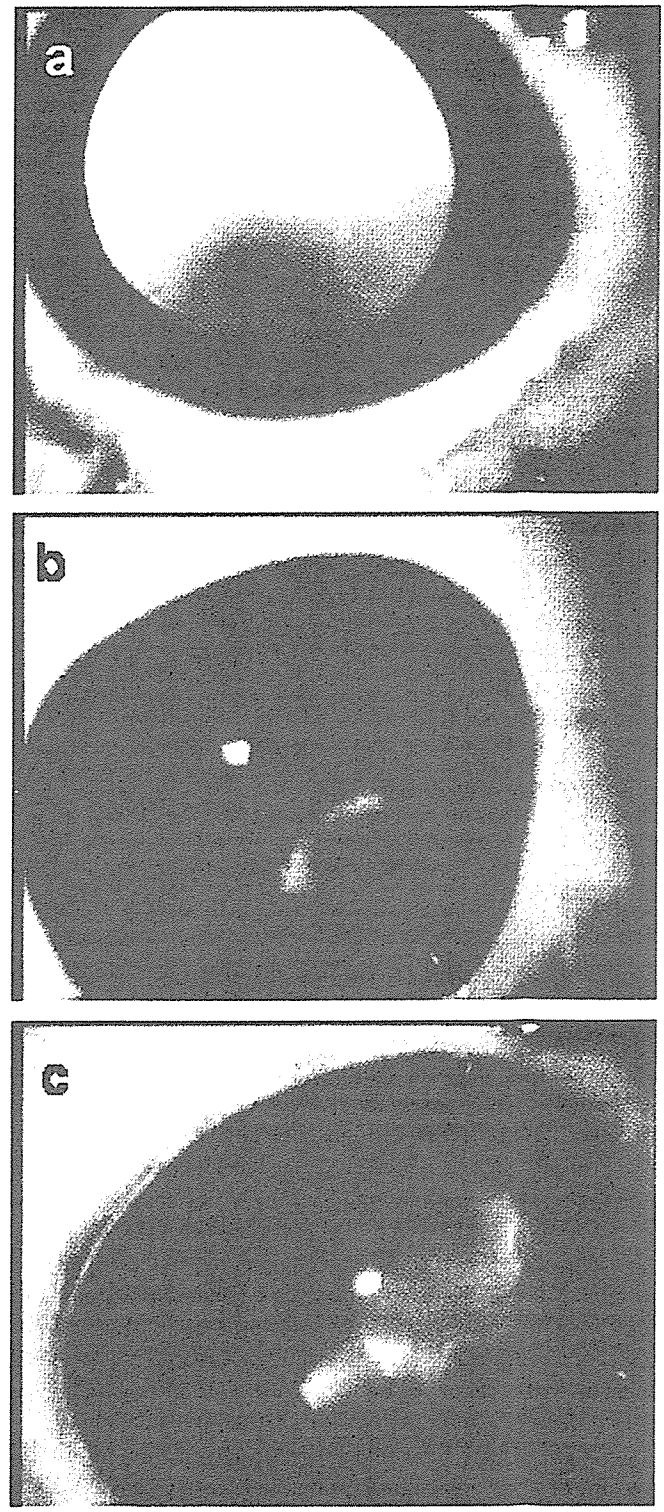

Fig. 3. Comparison of ACQDs and conventional organic dyes to perform vitrectomy. A vitrectomy of the porcine eye (6 months old) was performed with: (a) fluorescein sodium; (b) indocyanine green; and (c) ACQDs. (a) The brighter fluorescence emitted from fluorescein sodium made it harder to observe the vitreous. (b) Indocyanine green illuminates only the narrow range. (c) ACQDs can visualize the structure of vitreous at a striking contrast. In the case of vitrectomy, transparent vitreous was stained. Then these dyes were excited by light guide to make a striking contrast in vitreous.

is an efficient dye for vitrectomy. Transparent vitreous stained red with ACQDs made it easy to cut and aspirate the target lesion completely (see supplementary movie S2). The translucent red fluorescence from ACQDs enabled us to confirm the

location of other structures such as the retina, blood vessels of retina, and ciliary body, and that resulted in reducing the risk to injure other eye structures [Fig. 3(c)]. In addition, the shaving of the surface of retina was required to complete vitrectomy. Visible and translucent ACQDs make it possible to complete vitrectomy successfully.

IV. Discussions

Currently, colloidal nanocrystal quantum dots (QDs) are widely used in biological and medical study because QDs are attractive fluorophores for multicolor imaging due to their broad absorption and narrow emission spectra, and brighter and higher photostability than organic dyes. Many advanced improvements on surface modification of QDs enable us to promote a lot of biological experiments. We previously reported that QDs were applied to some biological experiments; long-term multicolor cell imaging in live cells [16]–[20], and even in cancer immunotherapy with QDs [21], [22]. In addition, this study suggests that ACQDs are excellent imaging agents to visualize invisible vitreous in clinical situations.

Although there are some concerns about the safety of ACQDs [23], we previously reported that the ACQD-covering molecules controlled their cytotoxicity unless the core structure of QDs was broken [24]. In vitrectomy, the ACQDs in vitreous were depleted completely by aspiration; then residual ACQDs were thought to be quite little after vitrectomy. We anticipate that the new imaging agent and method will be used broadly, and that vitreous conditions will be diagnosed and understood easily and fully in usual clinical situations. And safe vitrectomy can be completed by any ophthalmic surgeons. With the development of *in vivo* imaging systems, ACQD techniques may contribute not only to analyzing the mechanism of the side effect but to producing new medicines in the future.

In this paper, we examined study with QDs medicine of CdSe/ZnS *in vivo*. Derfus *et al.* [25] reported that core-shell typed QDs irradiated with ultraviolet more than 8 h showed the cytotoxicity by the leaked Cd^{2+} ion, but no sign of cytotoxicity in case of 1 hr exposure. We also found no sign of cytotoxicity under the condition of our *in vitro* experiments with some epithelial cell lines. In addition, no significant change was observed in vitreous after a wide range of doses of the ACQDs *in vivo*. This result is consistent with the report of Derfus *et al.* QDs made from metals that could generate toxic ions might exhibit cytotoxicity in some unexpected cases. Warner *et al.* reported the method of the production of silicon dots [26]. Further study will make possible clinical applications of QDs made from materials more suitable for safety, such as silicon.

V. Conclusion

ACQDs are much better imaging reagents in vitreous compared with some conventional dyes used in clinical situations. ACQDs will enable ophthalmic surgeons to perform more reliable vitrectomy, resulting in an easy and safe surgery method. Consequently, an ACQD-oriented vitreous system will light the way for ophthalmological science and clinical treatment.

Acknowledgment

The authors would like to thank Japan Alcon Corporation (Tokyo, Japan) for kindly providing a three port pars plana vitrectomy system. The authors are also grateful to Dr. M. Nii (Tokushima A. F. F. Technology Center, Tokushima Japan) for kindly providing an aged porcine eye.

References

[1] J. G. F. Worst and L. I. Los, *Cisternal Anatomy of the Vitreous*. The Hague, The Netherlands: Kugler, 1995.
[2] J. Sebag, "Anomalous posterior vitreous detachment: a unifying concept in vitreo-retinal disease," *Grafe's Arch. Clin. Exp. Ophthalmol.*, vol. 242, pp. 690–698, 2004.
[3] ——, "Age-related changes in human vitreous structure," *Graefes Arch Clin Exp Ophthalmol*, vol. 225, pp. 89–93, 1987.
[4] ——, "Seeing the invisible: the challenge of imaging vitreous," *J. Biomed. Opt.*, vol. 9, pp. 38–46, 2004.
[5] A. Kakehashi, S. Ishiko, S. Konno, J. Akiba, M. Kado, and A. Yoshida, "Observing the posterior vitreous by means of the scanning laser ophthalmoscope," *Arch. Ophthalmol.*, vol. 113, pp. 558–560, 1995.
[6] D. J. Coleman, S. W. Daly, A. Atencio, H. O. Lloyd, and R. H. Silverman, "Ultrasonic evaluation of the vitreous and retina," *Semin. Ophthalmol.*, vol. 13, pp. 210–218, 1998.
[7] T. Hikichi, J. Akiba, A. Kakehashi, and A. Yoshida, "Vitreous observation using a CCD camera and a computerized unit for image processing and storage," *Retina*, vol. 15, pp. 505–507, 1995.
[8] K. Mori and S. Yoneya, "Enhanced documentation of slit-lamp images of the human vitreous stained with fluorescein sodium," *Ophthalmic Surg. Lasers Imaging*, vol. 35, pp. 233–238, 2004.
[9] W. Drexler, U. Morgner, R. K. Ghanta, F. X. Kartner, J. S. Schuman, and J. G. Fujimoto, "Ultrahigh-resolution ophthalmic optical coherence tomography," *Nature Med.*, vol. 7, pp. 502–507, 2001.
[10] M. W. Johnson, "Improvements in the understanding and treatment of macular hole," *Curr. Opin. Ophthalmol.*, vol. 13, pp. 152–160, 2002.
[11] V. Tanner, D. S. Chauhan, T. L. Jackson, and T. H. Williamson, "Optical coherence tomography of the vitreoretinal interface in macular hole formation," *Br J Ophthalmol*, vol. 85, pp. 1092–1097, 2001.
[12] H. Terasaki, Y. Miyake, M. Mori, T. Suzuki, and M. Kondo, "Fluorescein angiography of extreme peripheral retina and rubeosis iridis in proliferative diabetic retinopathy," *Retina*, vol. 19, pp. 302–308, 1999.
[13] J. K. Challa, M. C. Gillies, P. L. Penfold, J. F. Gyory, A. B. Hunyor, and F. A. Billson, "Exudative macular degeneration and intravitreal triamcinolone: 18 month follow up," *Aust. N. Z. J. Ophthalmol.*, vol. 26, pp. 277–281, 1998.
[14] J. B. Jonas, I. Kreissig, and R. Degenring, "Intraocular pressure after intravitreal injection of triamcinolone acetonide," *Br. J. Ophthalmol.*, vol. 87, pp. 24–27, 2003.
[15] D. M. Moshfeghi, P. K. Kaiser, I. U. Scott, J. E. Sears, M. Benz, J. P. Sinesterra, R. S. Kaiser, S. J. Bakri, R. K. Maturi, J. Belmont, P. M. Beer, T. G. Murray, H. Quiroz-Mercado, and W. F. Mieler, "Acute endophthalmitis following intravitreal triamcinolone acetonide injection," *Amer. J. Ophthalmol.*, vol. 136, pp. 791–796, 2003.
[16] M. Dahan, S. Levi, C. Luccardini, P. Rostaing, B. Riveau, and A. Triller, "Diffusion dynamics of glycine receptors revealed by single-quantum dot tracking," *Science*, vol. 302, pp. 442–445, 2003.
[17] E. R. Goldman, A. R. Clapp, G. P. Anderson, H. T. Uyeda, J. M. Mauro, I. L. Medintz, and H. Mattoussi, "Multiplexed toxin analysis using four colors of quantum dot fluororeagents," *Anal. Chem.*, vol. 76, pp. 684–688, 2004.
[18] A. Hoshino, K. Fujioka, T. Oku, S. Nakamura, M. Suga, Y. Yamaguchi, K. Suzuki, M. Yasuhara, and K. Yamamoto, "Quantum dots targeted to the assigned organelle in living cells," *Microbiol. Immunol.*, vol. 48, pp. 985–994, 2004.
[19] J. K. Jaiswal, H. Mattoussi, J. M. Mauro, and S. M. Simon, "Long-term multiple color imaging of live cells using quantum dot bioconjugates," *Nature Biotechnol.*, vol. 21, pp. 47–51, 2003.
[20] A. Hoshino, K. Hanaki, K. Suzuki, and K. Yamamoto, "Applications of T-lymphoma labeled with fluorescent quantum dots to cell tracing markers in mouse body," *Biochem. Biophys. Res. Commun.*, vol. 314, pp. 46–53, 2004.
[21] X. Gao, Y. Cui, R. M. Levenson, L. W. Chung, and S. Nie, "In vivo cancer targeting and imaging with semiconductor quantum dots," *Nature Biotechnol.*, vol. 22, pp. 969–976, 2004.